Predictive control of flow rates and concentrations in sewage networks

Shuyao Tan, Alain Rapaport, Peter A. Vanrolleghem, Denis Dochain, Elodie Passeport, Joshua A. Taylor

Predictive control of flow rates and concentrations in sewage networks

Shuyao Tan[a], Alain Rapaport[b], Peter A. Vanrolleghem[c], Denis Dochain[d], Elodie Passeport[e], Joshua A. Taylor[f]

[a] *University of Toronto, Toronto, ON, Canada*
[b] *MISTEA, University Montpellier, INRAE, Institut Agro, 34060 Montpellier, France*
[c] *ModelEAU, Université Laval, Québec, QC, Canada*
[d] *ICTEAM, UCLouvain, 4-6 avenue Georges Lemaître, 1348 Louvain-la-Neuve, Belgium*
[e] *Rutgers University, New Brunswick, NJ, USA*
[f] *New Jersey Institute of Technology, Newark, NJ, USA*

Abstract

We design a predictive flow rate and concentration controller for wastewater transport and treatment networks. It manages flow rates to avoid overflows during times of high flow, and maximizes treatment efficiency when the system is within capacity limits. The underlying optimization is nonlinear due to the microbial growth kinetics and bilinear mass flows. Using a second-order cone relaxation of the microbial growth constraints and the alternating direction method of multipliers, we break down the problem into second-order cone and quadratic programs. This allows us to solve the problem at large scales in real-time. In a case study based on the wastewater transport and treatment system in the City of Paris, our controller outperforms the conventional flowrate-based controller by removing 13.7% more pollutant mass while treating the same amount of wastewater.

Keywords: Wastewater treatment, sewer network, second-order cone programming, alternating detection method of multipliers, predictive control.

1. Introduction

Urban wastewater systems consist of the sewer network, the treatment plants, and the receiving environment. In a combined system, the sewer network collects and transports both stormwater and sanitary wastewater to the treatment plants. In many networks, actuators like pumps, gates, and valves help manage flow. Most systems today do so to minimize combined sewer overflow (CSO) and treatment bypasses. In principle, flows can also be managed to improve treatment efficiency, thus reducing pollutant emissions to the environment. This requires accounting for the biochemical processes in the plants, which are nonlinear and hence computationally challenging.

In this study, we design a new predictive controller for flow management in urban wastewater systems. Our controller is based on a nonlinear model with both flow rates and pollutant concentrations. During times of high flow, it minimizes overflow, and when the system is within capacity limits, it maximizes treatment efficiency.

The controller operates in receding horizon fashion, wherein the decision is re-optimized in each time period. The optimizations have two sources of nonlinearity: the microbial growth kinetics in the treatment plants, which are typically modeled by the Monod function, and bilinear mass flows. We handle the growth kinetics using the second-order cone (SOC) relaxation of [1]. We handle the bilinearity using the alternating direction method of multipliers (ADMM) [2]. This enables us to alternate between a quadratic program (QP) and an SOCP, both of which can be solved at large scales using commercial software.

In the existing literature, modeling and control of the sewer network and the treatment plant are often separate. Many sewer control studies model the plants as static outlets of the sewer network and do not account for their treatment processes. [3] This type of control can be categorized as volume or pollution-based [4]. Volume-based control manages flow rates in the sewer pipes so as to minimize CSO and bypasses [5, 6, 7]. For combined systems, untreated overflows to the streets and the receiving environment are significant pollution sources motivating work on CSO management [8, 9, 10]. Both static optimization and dynamic control strategies have been proposed, in some cases reducing CSO by 17% [11]. Pollution-based control improves the dry weather performance by also maximizing the pollutant mass arriving at the treatment plants in order to minimize pollutant discharge [12, 13]. However, this does not always optimize receiving water quality because it does not account for the treatment processes in the plants and interactions between plant effluents and the receiving environment [14]. Similarly, plant controllers neglect the sewer network, treating it as an inlet with un-

Email addresses: ellote.tan@mail.utoronto.ca (Shuyao Tan), alain.rapaport@inrae.fr (Alain Rapaport), peter.vanrolleghem@gci.ulaval.ca (Peter A. Vanrolleghem), denis.dochain@uclouvain.be (Denis Dochain), ep756@envsci.rutgers.edu (Elodie Passeport), jat94@njit.edu (Joshua A. Taylor)

certain flow rates and concentrations [15]. This has motivated several integrated, immission-based controllers that optimize receiving water quality by accounting for both the wastewater treatment system and the receiving environment [16, 17, 4]. Immission-based control can achieve better environmental protection, but it is more complex in that it requires nonlinear modeling and real-time monitoring of the receiving environment; integrated modeling of heterogeneous components; and extensive calibration and validation of parameters that can change over time [18, 19, 20, 21]. In this paper, we design a controller that incorporates a dynamic model of the biochemical processes in the treatment plants, similar to immission-based controllers. However, unlike immission-based systems, we do not model or monitor the receiving environment. Our controller is thus more similar to pollution-based methods, but with further modeling of the coupling between the sewer network and treatment plants.

The main novelty of our controller is its computational structure. By using a recent SOC relaxation of the microbial growth kinetics, we break down the problem into an QP for flows and an SOCP for concentrations. This enables us to solve problems with numerous variables and time periods in real-time. During times of high flow, the controller minimizes CSO and flooding, as with volume-based control; and during low flow, the controller minimizes pollutant discharge. We implement the controller in a case study based on the City of Paris wastewater transport and treatment network. Compared to a conventional, flowrate-based controller, our controller releases 13.7% less pollutant mass while treating the same volume of wastewater.

The rest of the paper is organized as follows. In Section 2, we describe the model and setup. In Section 3, we formulate the flow management optimization with convex relaxation, and its solution via ADMM. In Section 4, we implement the optimization within a model predictive controller. In Section 5, we evaluate the performance of the controller in a case study based on the City of Paris wastewater transport and treatment network.

2. Modeling

2.1. Network

The network consists of n tanks interconnected by pipes. The tanks can be real or virtual. Real tanks can be storage in the pipe network, or reactors in the treatment plants. Virtual tanks represent the volume of sewage pipelines within a catchment area. The volume stored in tank i is denoted V_{ii}, and $V \in \mathbb{R}^{n\times n}$ is a diagonal matrix of the volumes. Actuators such as valves and pumps are represented by their corresponding flow rates. We use $Q_i^{\text{in}} \in \mathbb{R}_+$ to denote the flow rate entering tank i from outside the network, $Q_i^{\text{out}} \in \mathbb{R}_+$ the flow rate exiting the network from tank i, and $Q_{ij} \in \mathbb{R}$ the flow rate from tank i to tank j. If tank i is not connected to outside, Q_i^{in} and Q_i^{out} can be zero.

Define the $n \times n$ matrices

$$C_{ij}(Q) = \begin{cases} 0, & i \neq j \\ Q_i^{\text{in}}, & i = j \end{cases}$$

$$M_{ij}(Q) = \begin{cases} Q_{ji}, & i \neq j \\ -Q_i^{\text{out}} - \sum_{k=1}^n Q_{ik}, & i = j, \end{cases}$$

and let $\bar{M}(Q) = \text{diag}[M(Q)\cdot\mathbb{1}]$ where $\mathbb{1}$ is a column of ones. $M(Q)$ is a compartmental matrix, and therefore, assuming the network is outflow connected, is negative definite. Assuming constant density, the evolution of the tank volumes is

$$\frac{dV}{dt} = C(Q) + \bar{M}(Q), \tag{1}$$

with initial volumes $V(0) = V_0$.

2.2. Biological Treatment

There are m components (substrates/biomasses) in each tank. Let $\xi_i \in \mathbb{R}_+^m$ denote the process state of tank i, which contains the substrate and biomass concentrations, and let $\xi_i^{\text{in}} \in \mathbb{R}_+^m$ be the corresponding influent concentrations. If tank i is not connected to outside, i.e. $Q_i^{\text{in}} = 0$, we take $\xi_i^{\text{in}} = 0$ just by convention.

There are r reactions in each reactor tank, which convert substrates to other substrates and biomasses. Let $\phi_i(\xi_i) \in \mathbb{R}_+^r$ be the reaction rate vector of tank i. Two commonly used kinetics models are the Monod [22] and Contois [23] growth rates. They model the kinetics of one microbial species of concentration x on a single limiting substrate of concentration s:

$$\mu_{\text{Monod}} = \mu^{\text{m}} \frac{sx}{k+s} \quad \text{and} \quad \mu_{\text{Contois}} = \mu^{\text{c}} \frac{sx}{kx+s}$$

where μ^{m}, μ^{c}, and k are constant parameters. Let $\kappa_i \in \mathbb{R}^{m\times r}$ be the stoichiometric matrix, which is all zeros if no reaction takes place in tank i, or if the reactions in tank i are negligible compared to other ones.

The dynamics in tank i, $i = 1, ..., n$, are:

$$\begin{aligned} \frac{d(V_{ii}\xi_i)}{dt} &= \frac{dV_{ii}}{dt}\xi_i + V_{ii}\frac{d\xi_i}{dt} \\ &= V_{ii}\kappa_i\phi_i(\xi_i) - Q_i^{\text{out}}\xi_i - \sum_{k=1}^n Q_{ik}\xi_i \\ &\quad + Q_i^{\text{in}}\xi_i^{\text{in}} + \sum_{k=1}^n Q_{ki}\xi_k. \end{aligned}$$

Define the stacked vectors $\xi = [\xi_1, ..., \xi_n]^\top$ and $\phi(\xi) = [\phi_1(\xi_1), ..., \phi_n(\xi_n)]^\top$. Let K be a block diagonal matrix with $\kappa_1, ..., \kappa_n$ on its main diagonal. Let $\hat{A} = A \otimes I_m$, where $\otimes$ represents the Kronecker product and $I_m \in \mathbb{R}^{m\times m}$ is the identity matrix. The dynamics of the concentrations can be written as:

$$\frac{d\hat{V}}{dt}\xi + \hat{V}\frac{d\xi}{dt} = \hat{V}K\phi(\xi) + \hat{M}(Q)\xi + \hat{C}(Q)\xi^{\text{in}}, \quad (2)$$

with initial concentrations $\xi(0) = \xi_0$.

2.3. Discretization and Time Delays

We discretize (1) and (2) to make them compatible with finite-dimensional optimization. Here we use a simple Euler step, but note that a more complicated scheme, e.g., Runge-Kutta, can also be used so long as it is linear. Here we also introduce time delays in the concentrations due to transit through the pipes.

Let there be τ time periods and constant time step Δ. For clarity, we slightly abuse notation and omit the time step from variable arguments, e.g., $V(t)$ is the matrix of volumes at time Δt. Define $D_t[f(\cdot)] = (f(t+1) - f(t))/\Delta$. The discretization of (1) is:

$$D_t[V(\cdot)] = C(Q(t)) + \bar{M}(Q(t)), \quad t = 0, ..., \tau - 1.$$

Denote the time delays as $d_k \in \mathbb{N}$, $k \in \mathcal{D}$. The discretization of (2), with time delay, is:

$$\begin{aligned}\hat{V}(t)D_t\left[\xi(\cdot)\right] + D_t\left[\hat{V}(\cdot)\right]\xi(t) = \hat{V}(t)K\phi(\xi(t)) \\ + \sum_{k\in\mathcal{D}}\Big(\hat{M}_k(Q(t))\xi(t-d_k) \\ + \hat{C}_k(Q(t))\xi^{\text{in}}(t-d_k)\Big),\end{aligned}$$

for $t = 0, ..., \tau - 1$. The matrices $\hat{M}_k$ and $\hat{C}_k$ specify which flows in the current time period carry which concentrations from earlier time periods. Mass conservation in continuous completely mixed tanks implies that

$$\begin{aligned}\sum_{k\in\mathcal{D}}\hat{M}_k(Q(t)) &= \hat{M}(Q(t)) \\ \sum_{k\in\mathcal{D}}\hat{C}_k(Q(t)) &= \hat{C}(Q(t))\end{aligned}$$

for $t = 0, ..., \tau - 1$. The initial conditions for delayed concentrations are $\xi(t) = \xi_t$, with $t = -\max_k d_k, ..., 0$, which is the range of time delays.

3. Optimization

We now formulate a general optimization problem for managing the sewage network. We first introduce the vector variable $T(t)$, which we constrain to be equal to the vector of kinetics, $\phi(\xi(t))$. This enables the convex relaxation in Section 3.3. We denote the objective $\mathcal{F}$ and constraints on concentrations, Ω_1, and flow rates, Ω_2, which we describe in Sections 3.1 and 3.2. The full optimization is below.

$$\begin{aligned}\min_{\xi,T,V,Q}\quad & \mathcal{F}(\xi, T, V, Q) && (3a)\\ \text{s.t.}\quad & T(t) = \phi(\xi(t)) && (3b)\\ & D_t[V(\cdot)] = C(Q(t)) + \bar{M}(Q(t)) && (3c)\\ & \hat{V}(t)D_t[\xi(\cdot)] + D_t\left[\hat{V}(\cdot)\right]\xi(t) = \hat{V}(t)KT(t) \\ & \quad + \sum_{k\in\mathcal{D}}\Big(\hat{M}_k(Q(t))\xi(t-d_k) \\ & \quad + \hat{C}_k(Q(t))\xi^{\text{in}}(t-d_k)\Big) && (3d)\\ & (\xi, T) \in \Omega_1,\ (Q, V) \in \Omega_2 && (3e)\\ & \quad t = 0, ..., \tau - 1.\end{aligned}$$

We introduce some notation to describe $\mathcal{F}$, Ω_1, and Ω_2. The following are subsets of the tanks.

- $\mathcal{P}$, the treatment plants.
- $\mathcal{V}$, the virtual tanks.
- $\mathcal{R}$, the real tanks.
- $\mathcal{U}$, the tanks whose outflow is uncontrolled.

The following are subsets of other constitutive elements in the sewage network.

- $\mathcal{A}$, the subset of active flow control devices, such as valves, gates, and weirs.
- $\mathcal{J}$, the subset of junctions with zero volumes.

3.1. Objectives

$\mathcal{F}(\xi, T, V, Q)$ can consist of multiple terms representing different control objectives, some of which are listed below. The first objective involves concentrations and flows, and the rest only flows. Different weights can be assigned to each term according to priority. Squaring the terms in the objective can improve numerical performance and discourage more extreme outcomes for each individual term.

- *Flooding.* When raining, the sewer network can saturate, and excess wastewater can flow onto streets. The corresponding objective term is

  $$\sum_{t=1}^{\tau} Q_{\text{f}}(t)^\top \mathbb{1},$$

  where $Q_{\text{f}}(t)$, the vector of flooding flows, is defined in Section 3.2.

- *Combined sewer overflow (CSO).* When raining, a part of the flow can bypass the treatment plant di-

rectly to the environment. The corresponding objective term is

$$\sum_{t=1}^{\tau} Q_{\text{CSO}}(t) = \sum_{t=1}^{\tau} \sum_{i \in \mathcal{P}} \max \left(Q_i^{\text{in}}(t) + \sum_{j=1}^{n} Q_{ji}(t) - Q_i^{\max}, 0 \right),$$

where $Q_i^{\max}$ is the maximum allowed flow rate into plant i.

- *Pollutant release.* We can improve treatment efficiencies by optimally allocating wastewater over the plants. The corresponding objective term is

$$\sum_{t=1}^{\tau} \sum_{i \in \mathcal{P}} \left(Q_i^{\text{out}}(t) \xi_i(t) \right)^{\top} \mathbb{1} + \left(Q_{\text{CSO},i}(t) \xi_i^{\text{in}}(t) \right)^{\top} \mathbb{1}.$$

- *Total stored volume.* This objective aims to empty the sewer network to make space for future rain events. At each time period, the total stored volume is the trace of V.

- *Final state.* This objective encourages the system to end at a specific state. It could be an empty state which encourages the system to empty as quickly as possible, or it could be a set point which enables long-term stability. This objective is computed as the absolute difference between the final state of the system and the set point.

- *Control action smoothness.* Valves and pumps should be operated smoothly to minimize wear and tear. Since the actuators are represented by flow rates, this objective penalizes large changes between flows:

$$\sum_{t=1}^{\tau} \|Q(t) - Q(t-1)\|_2^2.$$

3.2. Constraints

The feasible set Ω_1 constrains the concentrations and reactions, and Ω_2 the flow rates and volumes. The following constraints make up Ω_1.

- Concentration limits of the form $0 \leq \xi(t) \leq \xi^{\text{reg}}$. This could represent regulatory limits on pollutant discharge from the treatment plants, $\mathcal{P}$.

- Initial concentrations, $\xi(t) = \xi_t$, $t = -\max_k d_k, ..., 0$.

Below are the constraints that make up Ω_2.

- Initial volumes, $V(0) = V_0$.

- The volume of wastewater stored in a real tank can not exceed its capacity:

$$0 \leq V_{ii}(t) \leq V_i^{\max}, \quad i \in \mathcal{R}.$$

- When the storage capacity of a virtual tank is exceeded, extra flow is either redirected to other tanks, or treated as overflow:

$$Q_{\text{f},i}(t) = \max\left((V_{ii}(t) - V_i^{\max}), 0\right), \quad i \in \mathcal{V}.$$

In the dynamics equations, $Q_{\text{f},i}$ is part of Q_i^{out}.

- Flow out from uncontrolled tanks driven by gravity is often approximated by a linear equation [24, 25, 26]:

$$Q_i^{\text{out}}(t) = \beta_i V_{ii}(t), \quad i \in \mathcal{U},$$

where β_i is a constant.

- Flow rate control devices such as valves, gates, and weirs are represented by the flow rate passing through the unit. Active units, such as controlled gates and valves, can manipulate the amount of flow passing through it within a certain range. The operational range can be a constant [7],

$$Q_i^{\min} \leq Q_i^{\text{out}}(t) \leq Q_i^{\max}, \quad i \in \mathcal{A},$$

or proportional to the stored volume [24, 25, 26]:

$$0 \leq Q_i^{\text{out}}(t) \leq \beta_i V_{ii}(t), \quad i \in \mathcal{A}. \tag{4}$$

- Flow rates are equal at junctions. At a junction, the volume is equal to zero:

$$V_{ii}(t) = 0, \quad i \in \mathcal{J}.$$

In this case, (2) simplifies to a mass balance equation.

3.3. Convex Relaxation

We relax constraint (3b) by changing the equality to inequality:

$$T(t) \leq \phi(\xi(t)). \tag{5}$$

The relaxation allows the microbial growth rate to be lower than its actual value. Since the optimization objective prioritizes maximizing the growth rate, the constraint remains tight in most cases. Let $T_r(t)$ be an element of $T(t)$ corresponding to a reaction with substrate $s(t)$ and biomass $x(t)$. In [1], it is shown that (5) has an SOC representation in the following two cases.

- If the growth rate is represented by the Contois function, then (5) takes the form

$$\left\| \begin{bmatrix} \mu^{\text{c}} s(t) \\ kT_r(t) \\ \mu^{\text{c}} kx(t) \end{bmatrix} \right\|_2 \leq \mu^{\text{c}} kx(t) + \mu^{\text{c}} s(t) - kT_r(t). \tag{6}$$

- If the growth rate is represented by the Monod function, and we assume that in each time period t, biomass is a fixed parameter, $x(t) = \bar{x}(t)$, then (5) takes the form

$$\left\| \begin{bmatrix} \mu^{\text{m}} s(t) \bar{x}(t) \\ kT_r(t) \\ \mu^{\text{m}} k\bar{x}(t) \end{bmatrix} \right\|_2 \leq \mu^{\text{m}} k\bar{x}(t) + \mu^{\text{m}} s(t) k - kT_r(t). \tag{7}$$

This relaxation can be tightened using a linear underestimator [1]. For example, the underestimator for the Monod kinetics model takes the form

$$T_r(t) \geq \underline{T_r}(t) + \left(\bar{T_r}(t) - \underline{T_r}(t)\right) \frac{s(t) - s^{\min}}{s^{\max} - s^{\min}},$$

where

$$\bar{T_r}(t) = \frac{\mu^{\mathrm{m}} s^{\max} \bar{x}(t)}{k + s^{\max}}, \underline{T_r}(t) = \frac{\mu^{\mathrm{m}} s^{\min} \bar{x}(t)}{k + s^{\min}},$$

and $s^{\min}$ and $s^{\max}$ are minimum and maximum concentrations. If such concentrations are not known, then we can use $s^{\min} = 0$ and $s^{\max}$ some large number. The relaxed optimization problem becomes:

$$\begin{aligned} \min_{\xi,T,V,Q} \quad & \mathcal{F}(\xi, T, V, Q) \\ \text{s.t.} \quad & (5),\ (3c) - (3e). \end{aligned} \tag{8}$$

3.4. Solution via ADMM

Problem (8) is difficult to solve due to the bilinearities between volumes, flow rates, and concentrations. We use ADMM, wherein we alternatively fix subsets of variables and solve the remaining subproblems [2]. Here, this means fixing flow rates and volumes while optimizing concentrations, an SOCP; and fixing concentrations while optimizing flow rates and volumes, a QP.

The scaled augmented Lagrangian is:

$$L(\xi, T, V, Q) = \mathcal{F}(\xi, T, V, Q) + \sum_{t=1}^{\tau} \frac{\rho}{2} ||E(t) + U(t)||_2^2,$$

where ρ is a small positive constant, U is the scaled dual variable, and

$$\begin{aligned} E(t) = & -\hat{V}(t) D_t[\xi(\cdot)] - D_t\left[\hat{V}(\cdot)\right] \xi(t) \\ & + \sum_{k \in \mathcal{D}} \Big(\hat{M}_k(Q(t)) \xi(t - d_k) \\ & + \hat{C}_k(Q(t)) \xi^{\mathrm{in}}(t - d_k) \Big) + \hat{V}(t) K T(t). \end{aligned}$$

For concision, we suppress the dependence on t below.

The ADMM consists of the following steps. The iterate is denoted by the superscript.

1. *Initialization.* Set $\alpha = 0$, $U(0) = \mathbf{0}$, and choose values for V^0, ξ^0, Q^0, and T^0. Note that only ξ^0 and T^0 need to be specified to proceed to Step 2, but specifying initial values of all variables can improve convergence.
2. *Solve.*

$$\begin{aligned} V^{\alpha+1}, Q^{\alpha+1} = \underset{V,Q}{\operatorname{argmin}} \quad & L\left(\xi^{\alpha}, T^{\alpha}, V, Q\right) \\ \text{s.t.} \quad & (3c) \\ & (Q, V) \in \Omega_2 \\ & t = 0, ..., \tau - 1. \end{aligned}$$

3. *Solve.*

$$\begin{aligned} \xi^{\alpha+1}, T^{\alpha+1} = \underset{\xi,T}{\operatorname{argmin}} \quad & L\left(\xi, T, V^{\alpha+1}, Q^{\alpha+1}\right) \\ \text{s.t.} \quad & (5) \\ & (\xi, T) \in \Omega_1 \\ & t = 0, ..., \tau - 1. \end{aligned}$$

4. *Update.*

$$U^{\alpha+1} = U^{\alpha} + E^{\alpha+1}.$$

5. *Termination.* If a termination criterion is satisfied, return the current solution. The termination criterion could be, e.g., maximum iterations or convergence of the objective, solution, or E. If a termination criterion is not satisfied, set $\alpha \leftarrow \alpha + 1$ and go to Step 2.

We note that ADMM is not guaranteed to converge to a local solution on bi-convex problems like (8). However, it is known to achieve good empirical performance, and does so in our examples. It is also relatively user-friendly in that it relies on convex solvers, and thus does not require the calculation of gradients and Hessians, which we acknowledge is now also a feature in several general nonlinear programming solvers.

4. Model Predictive Control

We implement the optimization via model predictive control (MPC). We note that this is more precisely economic MPC, wherein the controller aims to minimize a cost and not necessarily to drive the state to equilibrium [27, 28]. Informally, MPC operates by applying the decisions in the first period; updating the parameters and pushing the time horizon back one period; resolving; and then again applying the decisions in the new first period [29]. Some of the benefits of MPC are that it incorporates uncertainty by updating the parameters in each iteration; it is computationally tractable because we can choose the time horizon; and it accommodates constraints. Although our controller does not guarantee stability, using a long prediction horizon and incorporating a final state (terminal) cost can still promote closed-loop stability.

Our MPC procedure is as follows. Let H be the horizon length and t_0 be the current time period.

1. *Forecasting and state estimation.* Obtain inlet vectors Q^{in} and ξ^{in} for $t = t_0, ..., t_0 + H - 1$. There are several techniques for forecasting inflow profiles, such as in [30], [31], and [32]. Also, obtain $\xi(t_0 - d_k)$, $k \in \mathcal{D}$, and $V(t_0)$ for initial conditions. These can be obtained by SCADA measurements, or using state estimators such as the Unscented Kalman Filter, a particle filter, or a moving horizon state estimator [33]. The forecasts and current state estimates are used to parameterize (8).

2. *Optimization.* Solve (8) over time periods $t = t_0, ..., t_0 + H - 1$. We do so using ADMM, as described in Section 3.4.
3. *Implementation.* Execute decisions for the current time period, t_0.
4. *Continuation.* Set $t_0 \to t_0 + 1$ and go to Step 1.

To speed up Step 2, we use the optimal solution of the current time period as the starting point for the next. More precisely, suppose $(V^*(t), Q^*(t), \xi^*(t), T^*(t))$, $t = t_0, ..., T_0 + H - 1$ is the solution at time t_0. In the next time period, $t_0 + 1$, the starting point for the ADMM routine is $(V^*(t), Q^*(t), \xi^*(t), T^*(t))$ for times $t = t_0+1, ..., t_0+H-1$. The starting point for the last period, $t_0 + H$, must be chosen by other means, e.g., equal to the starting point of the second last period, $t_0 + H - 1$.

5. Case Study

We now present results from a case study based on a part of the City of Paris (France) sewage network, shown in Figure 1.

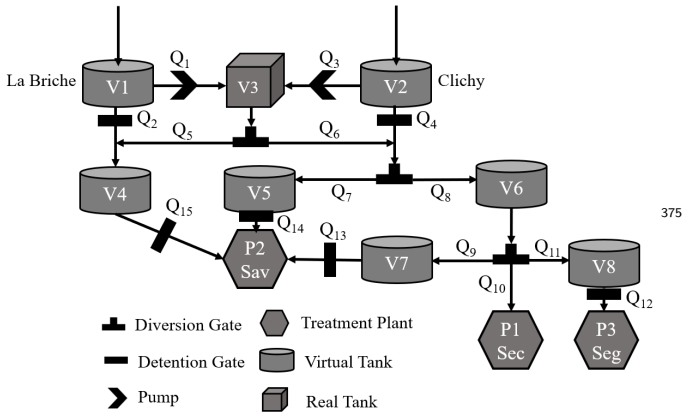

Figure 1: Simplified representation of the catchment area.

5.1. System Description

The network includes 8 tanks (7 virtual, 1 real) and 3 treatment plants. Volumes and time delays of the tanks are listed in Table 1. Time delays are estimated based on the total volume of each virtual tank and are assumed to be constant, independent of the flowrate. The time delays are due to the tanks, but are mathematically represented in the flows. Volumes and flow requirements of the treatment plants are listed in Table 2.

The tanks are connected by detention gates, diversion gates, and pumps. Detention gates and pumps are modelled as active units as in (4) with $\beta = 0.15$, and diversion gates are modelled as junctions.

The two input streams represent the Clichy and La Briche pre-treatment facilities. The Seine Centre (Sec), Seine Aval (Sav) and Seine Grésillons (Seg) treatment plants

	Volume (m^3)	Time delay (min)
V_1	1.6×10^5	60 (Q_1, Q_2)
V_2	8.0×10^4	30 (Q_3, Q_4)
V_3	8.0×10^4	30 (Q_5, Q_6)
V_4	8.0×10^4	30 (Q_{15})
V_5	1.2×10^5	45 (Q_{14})
V_6	8.0×10^4	30 (Q_9, Q_{10}, Q_{11})
V_7	4.0×10^4	15 (Q_{13})
V_8	1.2×10^5	45 (Q_{12})

Table 1: Volumes and time delays of the tanks. The corresponding flows are listed in parentheses.

	Volume (m^3)	$Q^{\min}$ ($m^3\,d^{-1}$)	$Q^{\max}$ ($m^3\,d^{-1}$)
P_1	2.0×10^4	4.8×10^4	2.4×10^5
P_2	1.6×10^5	1.4×10^5	1.7×10^6
P_3	3.0×10^4	1.9×10^4	1.0×10^5

Table 2: Volumes and flow requirements of the plants.

are modelled as reactors with constant volumes. The following constraint is added to Ω_2:

$$Q_i^{\text{in}}(t) + \sum_{j=1}^{n} Q_{ji}(t) = Q_i^{\text{out}}(t), \quad i \in \mathcal{P}.$$

At each treatment plant, the dynamics of biochemical oxygen demand (BOD), ammonia nitrogen (NH_4^+), nitrite nitrogen (NO_2^-), and nitrate nitrogen (NO_3^-) are modelled assuming Monod growth rates with constant biomass at $\bar{x}(t) = 1 \times 10^3$ (mg L^{-1}). The vector of concentrations is thus

$$\xi = \left[S^{\text{BOD}}, S^{\text{NH}_4^+}, S^{\text{NO}_2^-}, S^{\text{NO}_3^-}\right]^\top.$$

Following [34], it is assumed that the air supply is sufficient for microbial growth, and pH in the plants is always around neutral pH. The corresponding parameters are listed in Table 3, which come from Table 1 in [34]. The stoichiometric matrix κ_i for each plant $i \in \mathcal{P}$ is:

Parameter	Sec	Sav	Seg
μ^{BOD} (d^{-1})	3.99	2.56	1.93
$\mu^{\text{NH}_4^+}$	0.84	0.83	0.89
$\mu^{\text{NO}_2^-}$	1.68	1.27	0.92
$\mu^{\text{NO}_3^-}$	1.21	1.38	0.85
k^{BOD} (mg L^{-1})	13.67	11.65	14.26
$k^{\text{NH}_4^+}$	6.59	14.98	8.53
$k^{\text{NO}_2^-}$	2.46	1.15	2.55
$k^{\text{NO}_3^-}$	1.40	2.69	4.20
$y^{\text{NH}_4^+,\ \text{NO}_2^-}$	0.28	0.25	0.27
$y^{\text{NO}_2^-,\ \text{NO}_3^-}$	0.68	0.64	0.70

Table 3: Growth rate parameters.

$$\kappa_i = \begin{bmatrix} -1 & 0 & 0 & 0 \\ 0 & -1 & 0 & 0 \\ 0 & 1/y_i^{\mathrm{NH}_4^+,\ \mathrm{NO}_2^-} & -1 & 0 \\ 0 & 0 & 1/y_i^{\mathrm{NO}_2^-,\ \mathrm{NO}_3^-} & -1 \end{bmatrix}.$$

Initial conditions of the system are listed in Table 4. The concentrations before time zero are assumed to be constant.

	Volume (m^3)	ξ ($\mathrm{mg\,L}^{-1}$)
V_1	6.4×10^4	$[128.9, 30.1, 0, 0]$
V_2	4.0×10^4	
V_3	0	
V_4	3.2×10^4	
V_5	4.8×10^4	
V_6	1.6×10^4	
V_7	1.6×10^4	
V_8	4.0×10^4	
P_1	2.0×10^4	$[5.0, 0.39, 10.2, 36.3]$
P_2	1.6×10^5	$[16.0, 6.8, 5.4, 40.0]$
P_3	3.0×10^4	$[2.5, 1.1, 0.7, 10.0]$

Table 4: Volumes and concentrations at time zero and before.

5.2. Controllers

All controller parameters are shown in Table 5. The termination criteria is set to 50 because the residual is the squared norm of a matrix with more than 6000 entries, and thus 50 does enforce near satisfaction of the soft constraint corresponding to each entry. The objective (8) consists of the following terms.

- *Pollutant release* (P). Total mass of discharged BOD, NH_4^+, NO_2^-, and NO_3^-.
- *Flooding and CSO* (F).
- *Total stored volume* (V).
- *Final volume* ($V(H)$). Total volume of wastewater stored in the system at the end of the optimization period compared to a set point value. The set point is computed by opening all valves over the horizon, and equally dividing the flows at diversion gates.

For the sake of comparison with a controller that does not model concentrations, we introduce the following term to promote balanced utilization of the treatment plants:

$$D = \sum_{t=1}^{\tau} \left(\frac{Q_i^{\mathrm{in}}(t)}{Q_i^{\max}(t)} - \frac{1}{\mathcal{P}} \sum_i \frac{Q_i^{\mathrm{in}}(t)}{Q_i^{\max}(t)} \right), \quad i \in \mathcal{P}.$$

We compare the performances of the following two controllers.

- *Flow rate controller (FC).* This aims to minimize flooding and CSO while evenly utilizing the treatment plants. It represents the present-day standard approach, and does not make use of concentrations.

$$\begin{aligned} \min_{V,Q} \quad & w_1 F^2 + w_2 V^2 + w_3 V(H)^2 + w_4 D^2 \\ \text{s.t.} \quad & (3c),\ (3e). \end{aligned} \tag{9}$$

- *Flow rate and concentration controller (FCC).* Our new controller aims to maximize treatment efficiency while avoiding flooding and CSO.

$$\begin{aligned} \min_{\xi,T,V,Q} \quad & w_1 F^2 + w_2 V^2 + w_3 V(H)^2 + w_5 P^2 \\ \text{s.t.} \quad & (5),\ (3c) - (3e). \end{aligned} \tag{10}$$

The values of the weights can be found in Table 5. Certain variables with inherently larger numerical values, such as volume and flow rates, must be scaled to make the terms comparable and to avoid numerical issues. Volumes are scaled down by a quarter of the average volume of all virtual tanks. Flows are scaled down by the average inlet flowrate. Concentrations are scaled down by the average inlet concentration. Squaring the objective terms makes these weights smaller yet. This is not an issue, as all of our computations are conducted with 16 digits of precision.

5.3. Simulations

The influent data is based on the Inf_rain_2006 dataset of [35] which contains two weeks of influent flow rates and concentrations at a 15-minute resolution. Inflow data for the first 2.5 days is used in our simulation. The inlet flow rate is scaled so that the average daily inflow is equivalent to 70% of the total treatment capacity $\left(\sum_{i\in\mathcal{P}} Q_i^{\max}\right)$ of the plants. The inlet flow rates of Tanks 1 and 2 are 60% and 40% of the total flow, respectively. Both tanks share the same inflow substrate state vector.

Three sets of simulations are conducted, and a summary of parameters can be found in Table 6.

- *Base case.* Problem (9) and (10) are solved with precise inlet profiles.
- *Smoothed case.* The control action smoothness objective (C) is added to (9) and (10).
- *Noisy case.* Gaussian noises (zero-mean, 0.1 standard deviation) are applied to the inlet profiles to simulate inaccurate predictions.

Decisions are made every 15 minutes, and flow variables evolve with a 15-minute time step. Concentrations evolve with a three-minute time step for better numerical precision. Flows are not on the three-minute discretization because volumes change relatively slowly, and the actuators receive new commands every 15 minutes.

Simulations were run in Matlab R2022a using CVX version 2.2 and the Gurobi solver version 9.00. [36, 37].

Objective weights	$w_1 = 1.00 \times 10^3$ $w_2 = 1.77 \times 10^{-9}$ $w_3 = 1.77 \times 10^{-7}$ $w_4 = 1.00 \times 10^3$ $w_5 = 1.55 \times 10^{-10}$ $w_6 = 1.77 \times 10^{-3}$
MPC parameters	$H = 6$ h $\Delta_{Q,V} = 15$ min $\Delta_\xi = 3$ min
Termination criteria	$\|\|E\|\|_2^2 \leq 50$
Penalty factor	$\rho = 0.1$

Table 5: Controller parameters.

Scenario	Objective function	Noise
Base	(9) (10)	None
Smoothed	(9) + $w_6 C^2$ (10) + $w_6 C^2$	None
Noisy	(9) (10)	Zero-mean, 0.1 standard deviation

Table 6: Parameters of simulation scenarios.

5.4. Results

The performance of FC and its improvement over FC in each scenario is summarized in Table 7. In Table 7, Q represents the total volume of wastewater treated by the plants (expressed in m^3), P represents the total mass of discharged pollutants (quantified in tons), and R represents the pollutants released (tons) that exceed the regulatory limit $[6, 0.5, 0.3, 50]$ mg L^{-1} for the concentrations of BOD, NH_4^+, NO_2^-, and NO_3^-, respectively. The percentage improvement is shown in parentheses next to FCC performance.

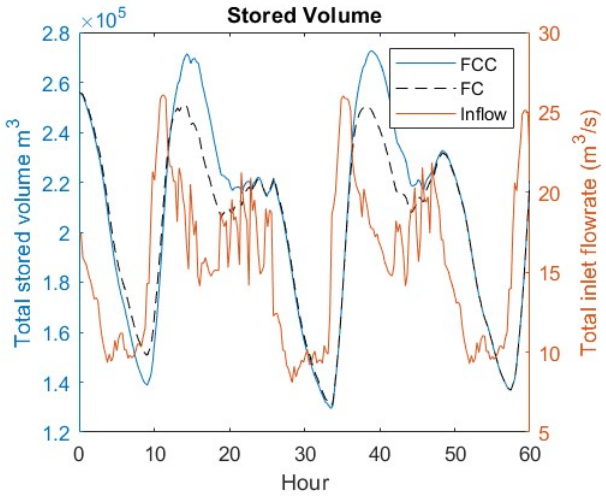

Figure 2: Total volume of wastewater stored in the system in the smoothed case.

Both controllers are effective in preventing flooding and CSO. FCC removes more pollutant mass while maintaining the same total wastewater flow as FC. This improvement results from better allocation of wastewater over the

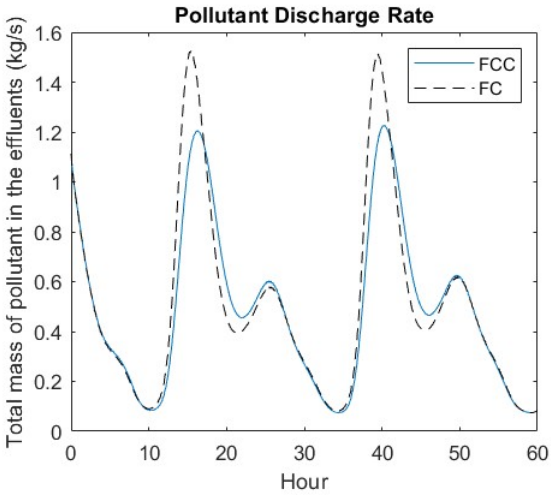

Figure 3: Pollutant discharge rate in the smoothed case.

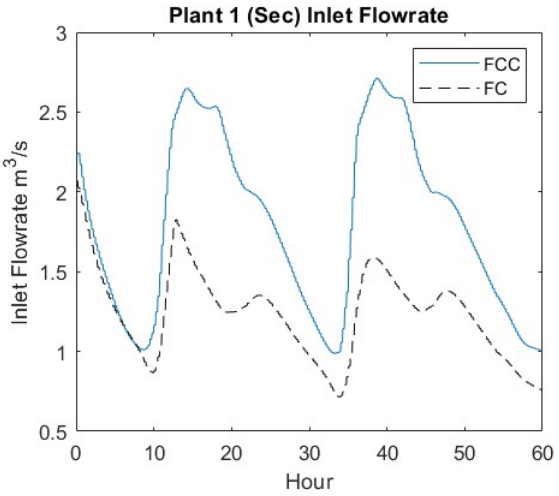

Figure 4: Plant 1 inlet flow rate in the smoothed case.

Scenario	Q (m^3)	P (tons)	R (tons)
Base	3.36×10^6 (same)	100 (−13.7%)	26.4 (−30.1%)
Smoothed	3.38×10^6 (same)	105 (−3.87%)	29.2 (−15.1%)
Noisy	3.33×10^6 (same)	112 (−3.83%)	30.7 (−18.8%)

Table 7: Performance of FCC and its improvement over FC in each scenario. Q represents total volume of treated wastewater, P represents the total mass of discharged pollutants, and R represents the pollutants released that exceed the regulatory limit.

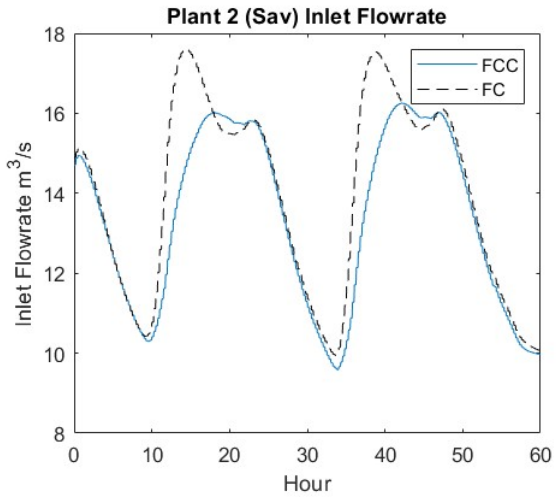

Figure 5: Plant 2 inlet flow rate in the smoothed case.

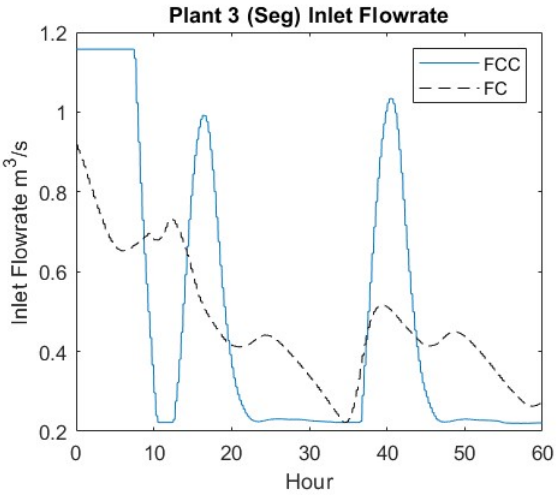

Figure 6: Plant 3 inlet flow rate in the smoothed case.

treatment plants, as depicted in Figures 2 to 6. During peak hours, FCC routes wastewater to Plants 1 and 3 instead of Plant 2. FCC also retains more wastewater in the sewage pipes during peak hours. This levels the load over time, enabling the plants to run more efficiently.

In the base case, FCC achieves a 14% decrease in discharged pollutants and a 30% reduction in regulation violation. There is a trade-off between control action smoothness and treatment efficiency, as shown in the second row of Table 7. Adding the control action smoothness term to the objective reduces the benefit of FCC. Nevertheless, FCC still outperforms FC, but to a lesser extent. In Figure 7, we see that adding the smoothness term to the objective results in substantially smoother control actions. As expected, adding noise to the inlet flow profiles degrades performance, but FCC still substantially outperforms FC.

The simulations were run on a personal laptop with an Intel i7-8750H CPU. It takes on average 2.5 minutes to solve the optimization problem for the 6-hour prediction horizon, which is within the 15-minute decision window. There are 24 time periods for flow variables, 120 time periods for concentration variables, and around 200 state variables in each time period. Each ADMM iteration has around 20000 variables with 15000 constraints. Typically around 10 iterations are needed to reach convergence. Figure 8 shows the convergence over five iterations. Note that while the residual decreases with each iteration, the objective might not, because early iterations might produce highly infeasible solutions. The warm-start procedure described in Section 4 reduces the number of iterations by roughly 80%. In each iteration, the SOCP step is typically three times slower than the QP step. If we shorten the time horizon to two hours, the average computation time becomes 50 seconds. These results demonstrate that the controller can be implemented in real-time.

6. Conclusion

We have developed a predictive flow rate and concentration controller for the wastewater transport and treatment network. It minimizes CSO, bypasses, and pollutant emissions in real-time. The City of Paris case study demonstrates that our controller releases 13% less pollutants than the conventional flow-based controller while treating the same amount of wastewater and avoiding CSO. The performance depends on the accuracy of the predicted inlet profile over the optimization horizon. Future work will focus on integrating inlet profile predictions, real-time

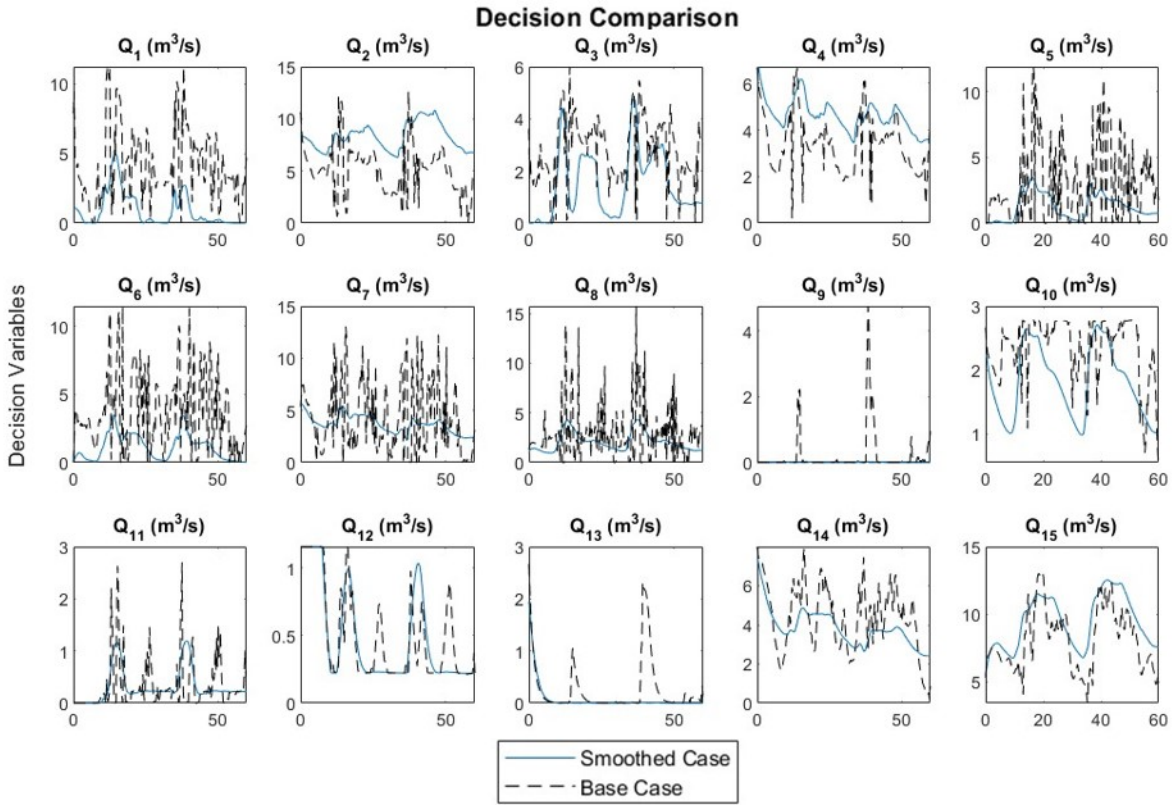

Figure 7: Control actions in the smoothed and base cases.

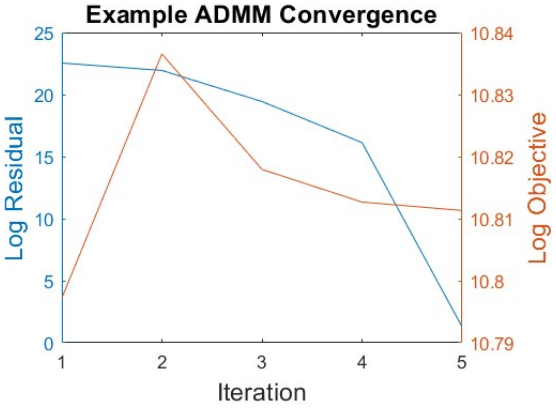

Figure 8: Example evolution of the residual and the objective value over iterations.

measurements and noises, and further improving computation so as to allow for longer horizons.

7. Acknowledgement

The authors would like to thank the research programme MOCOPEE (MOdélisation Contrôle et Optimisation des Procédés d'Epuration des Eaux) for its technical and scientific support. Peter Vanrolleghem's work was supported by the Natural Sciences and Engineering Research Council of Canada Discovery Grant RGPIN-2021-04347: towards digital twin based control of water resource recovery facilities - methods supporting the use of adaptive hybrid digital twins.

References

[1] J. Taylor, A. Rapaport, Second-order cone optimization of the gradostat, Computers & Chemical Engineering 151 (2021) 107347. doi:10.1016/j.compchemeng.2021.107347.

[2] S. Boyd, N. Parikh, E. Chu, B. Peleato, J. Eckstein, Distributed optimization and statistical learning via the alternating direction method of multipliers, Foundations and Trends in Machine Learning 3 (1) (2011) 1–122. doi:10.1561/2200000016.

[3] D. Butler, M. Schütze, Integrating simulation models with a view to optimal control of urban wastewater systems, Environmental Modelling & Software 20 (4) (2005) 415–426. doi:10.1016/j.envsoft.2004.02.003.

[4] P. Vanrolleghem, L. Benedetti, J. Meirlaen, Modelling and real-time control of the integrated urban wastewater system, Environmental Modelling & Software 20 (4) (2005) 427–442. doi:10.1016/j.envsoft.2004.02.004.

[5] G. Cembrano, J. Quevedo, M. Salamero, V. Puig, J. Figueras, J. Martı, Optimal control of urban drainage systems. a case study, Control engineering practice 12 (1) (2004) 1–9. doi:10.1016/S0967-0661(02)00280-0.

[6] C. Ocampo-Martínez, V. Puig, J. Quevedo, A. Ingimundarson, Fault tolerant model predictive control applied on the Barcelona sewer network, in: Proceedings of the 44th IEEE Conference on Decision and Control, 2005, pp. 1349–1354.

[7] U. Rathnayake, A. F. Anwar, Dynamic control of urban sewer systems to reduce combined sewer overflows and their adverse impacts, Journal of Hydrology 579 (2019) 124150. doi:10.1016/j.jhydrol.2019.124150.

[8] C. Ocampo-Martinez, Model predictive control of wastewater systems, Springer Science & Business Media, 2010.

[9] R. Burm, D. Krawczyk, G. Harlow, Chemical and physical comparison of combined and separate sewer discharges, Journal (Water Pollution Control Federation) (1968) 112–126.

[10] L. García, J. Barreiro-Gomez, E. Escobar, D. Téllez, N. Quijano, C. Ocampo-Martínez, Modeling and real-time control of urban drainage systems: A review, Advances in Water Resources 85 (2015) 120–132. doi:10.1016/j.advwatres.2015.08.007.

[11] A. Bachmann-Machnik, Y. Brüning, A. Ebrahim Bakhshipour, M. Krauss, U. Dittmer, Evaluation of combined sewer system operation strategies based on highly resolved online data, Water 13 (6) (2021) 751. doi:10.3390/w13060751.

[12] M. Mahmoodian, O. Delmont, G. Schutz, Pollution-based model predictive control of combined sewer networks, considering uncertainty propagation, International Journal of Sustainable Development and Planning 12 (1) (2017) 98–111. doi:10.2495/SDP-V12-N1-98-111.

[13] C. Sun, L. Romero, B. Joseph-Duran, J. Meseguer, E. Muñoz, R. Guasch, M. Martinez, V. Puig, G. Cembrano, Integrated pollution-based real-time control of sanitation systems, Journal of Environmental Management 269 (2020) 110798. doi:10.1016/j.jenvman.2020.110798.

[14] J. Lau, D. Butler, M. Schütze, Is combined sewer overflow spill frequency/volume a good indicator of receiving water quality impact?, Urban Water 4 (2) (2002) 181–189. doi:10.1016/S1462-0758(02)00013-4.

[15] R. Hreiz, M. Latifi, N. Roche, Optimal design and operation of activated sludge processes: State-of-the-art, Chemical Engineering Journal 281 (2015) 900–920. doi:10.1016/j.cej.2015.06.125.

[16] W. Rauch, P. Harremoes, The importance of the treatment plant performance during rain to acute water pollution, Water Science and Technology 34 (3) (1996) 1–8. doi:10.1016/0273-1223(96)00549-5.

[17] M. Schütze, D. Butler, M. B. Beck, Optimisation of control strategies for the urban wastewater system — an integrated approach, Water Science and Technology 39 (9) (1999) 209–216. doi:10.1016/S0273-1223(99)00235-8.

[18] H. Zhu, G. Huang, P. Guo, Sifnp: simulation-based interval-fuzzy nonlinear programming for seasonal planning of stream water quality management, Water, Air, & Soil Pollution 223 (2012) 2051–2072. doi:10.1007/s11270-011-1004-5.

[19] B. Joseph-Duran, J. Meseguer, G. Cembrano, T. Maruéjouls, A. Montserrat, M. Martínez, R. Guasch, P. Rouge, Life effidrain: efficient integrated real-time control in urban drainage systems for environmental protection, in: 14th International CCWI Conference, 2016.

[20] F. Meng, R. Saagi, Integrated modelling and control of urban wastewater systems, in: Water-Wise Cities and Sustainable Water Systems: Concepts, Technologies, and Applications, IWA Publishing, 2021. doi:10.2166/9781789060768_0259.

[21] P. M. Bach, W. Rauch, P. S. Mikkelsen, D. T. McCarthy, A. Deletic, A critical review of integrated urban water modelling – urban drainage and beyond, Environmental Modelling & Software 54 (2014) 88–107. doi:10.1016/j.envsoft.2013.12.018.

[22] J. Monod, The growth of bacterial cultures, Annual Review of Microbiology 3 (1) (1949) 371–394.

[23] D. Contois, Kinetics of bacterial growth: relationship between population density and specific growth rate of continuous cultures, Microbiology 21 (1) (1959) 40–50.

[24] C. Sun, L. Romero, B. Joseph-Duran, J. Meseguer, R. G. Palma, M. M. Puentes, V. Puig, G. Cembrano, Control-oriented quality modelling approach of sewer networks, Journal of environmental management 294 (2021) 113031. doi:10.1016/j.jenvman.2021.113031.

[25] A. Zimmer, A. Schmidt, A. Ostfeld, B. Minsker, Reducing combined sewer overflows through model predictive control and capital investment, Journal of Water Resources Planning and Management 144 (2) (2018) 04017091. doi:10.1061/(ASCE)WR.1943-5452.0000879.

[26] Y. Li, P. Voulgaris, D. Stipanović, Z. Gu, Decentralized model predictive control of urban drainage systems, WSEAS transactions on systems and control 14 (2019).

[27] J. B. Rawlings, D. Angeli, C. N. Bates, Fundamentals of economic model predictive control, in: 2012 IEEE 51st IEEE conference on decision and control (CDC), IEEE, 2012, pp. 3851–3861.

[28] M. Ellis, J. Liu, P. D. Christofides, Economic model predictive control, Springer 5 (7) (2017).

[29] E. F. Camacho, C. Bordons, Model predictive control, 2nd Edition, Springer, 2004.

[30] J. Chen, R. Ganigué, Y. Liu, Z. Yuan, Real-time multistep prediction of sewer flow for online chemical dosing control, Journal of Environmental Engineering 140 (11) (2014). doi:10.1061/(ASCE)EE.1943-7870.0000860.

[31] M. Ansari, F. Othman, T. Abunama, A. El-Shafie, Analysing the accuracy of machine learning techniques to develop an integrated influent time series model: case study of a sewage treatment plant, Malaysia, Environmental Science and Pollution Research 25 (12) (2018) 12139–12149. doi:10.1007/s11356-018-1438-z.

[32] F. Li, P. A. Vanrolleghem, An influent generator for WRRF design and operation based on a recurrent neural network with

multi-objective optimization using a genetic algorithm, Water Science and Technology 85 (5) (2022) 1444–1453. doi:10.2166/wst.2022.048.

[33] J. A. Taylor, A. Rapaport, D. Dochain, A sequential convex moving horizon estimator for bioprocesses, Journal of Process Control 116 (2022) 19–24. doi:10.1016/j.jprocont.2022.05.012.

[34] C. Robles-Rodriguez, J. Bernier, V. Rocher, D. Dochain, A simple model of wastewater treatment plants for managing the quality of the seine river, IFAC-PapersOnLine 51 (18) (2018) 880–885, 10th IFAC Symposium on Advanced Control of Chemical Processes. doi:10.1016/j.ifacol.2018.09.236.

[35] J. Alex, L. Benedetti, J. B. Copp, K. V. Gernaey, U. Jeppsson, I. Nopens, M.-N. Pons, J. P. Steyer, P. A. Vanrolleghem, Benchmark simulation model no. 1 (bsm1), The International Water Association, 2008.

[36] M. Grant, S. Boyd, CVX: Matlab software for disciplined convex programming, version 2.1, http://cvxr.com/cvx (2014).

[37] Gurobi Optimization, LLC, Gurobi Optimizer Reference Manual (2023).